Supplementary Material for

Riverine supply to the eastern Mediterranean during last interglacial sapropel S5 formation: a basin-wide perspective

Jiawang Wu [a,b *], Amalia Filippidi [a], Gareth R. Davies [c], and Gert J. de Lange [a,b]

[a] Department of Earth Sciences–Geochemistry, Faculty of Geosciences, Utrecht University, Princetonplein 9, 3584 CC Utrecht, The Netherlands

[b] State Key Laboratory of Marine Geology, Tongji University, Siping 1239, 200092 Shanghai, China

[c] Department of Petrology, Faculty of Earth and Life Sciences, Vrije Universiteit (VU) Amsterdam, De Boelelaan 1085, 1081 HV Amsterdam, The Netherlands

[*] Corresponding author.

E-mail address: j.w.wu@uu.nl (J. Wu).

Submitted to

Chemical Geology, 2018

This **Supplementary Material** provides 1) a compiled dataset of Sr and Nd isotopes for surface sediments in the eastern Mediterranean Sea (EMS) and detailed data sources of Sr and Nd isotopes for sapropel S1, as well as 2) a description of the semi-quantitate estimates for the major provenance areas over the EMS.

1 Data sources

In Table S1, an updated Sr-Nd isotope dataset of EMS surface sediments is given, including published data and the data from this study. The data are regionally grouped to better indicate the present-day situation (Figures 2 and 6 in manuscript).

For the Sr and Nd isotopes data of sapropel S1, averaged values are reported for each core/site (Table S2), as shown in Figures 2 and 6 of the manuscript. The interval of sapropel S1 is based on the well-established age boundaries (10.8–6.1 ± 0.5 cal. ka; De Lange et al., 2008). Specifically, in Figure 2 of the manuscript, data of representative cores taken from the main provenance are shown for the Holocene. This is indicative of the influences of different riverine contributions over sapropel S1, i.e. the domain of Libyan-Tunisian paleodrainage fluxes (after core CP10; Wu et al., 2016), NBEM riverine inputs (after cores SL114 and BC03; Freydier et al., 2001; Wu et al., 2016), and Nile discharge (after cores BC19, MS27, and BC07; Freydier et al., 2001; Revel et al., 2010; 2014).

2 Semi-quantitative estimates

As discussed in Section 4 of the manuscript, for the three provenance areas the major detrital contributions are different, which makes a quantitative calculation for the whole EMS basin challenging. This is particularly true in view of the overlapping isotopic signatures between the Nile and Aegean riverine contributions, the complex provenance pattern of the Ionian Sea, as well as the inadequate information for the source endmembers (e.g. detrital Mg for Adriatic and Aegean). Despite these limitations, semi-quantitative estimates can be made for the different major provenance areas. This is done on the basis of some qualified assumptions concerning the distribution of detrital river-borne materials (see Section 4 of the manuscript).

For the Levantine Basin, the mixing hyperbola constructed on the basis of Sr and Nd isotopes and concentrations (after Revel et al., 2010), allows us to quantify the Nile vs. Saharan contributions (Figure S1). This is adopted because the study of Revel et al. (2010) compiled various Nile-associated samples over the past 100 ka, which provides a comprehensive and direct comparison for the detrital Sr-Nd isotope data. The comparison is based on the assumption of a simple mixing between Nile sediment and Saharan dust in the Levantine Basin. The Nile contribution ranges between 40–70% during humid sapropel periods (i.e. Holocene sapropel S1, MIS 3, and last-interglacial sapropels S3 and S4). By contrast, the Nile contribution could fall to ~15% at least and the Saharan dust

contribution could reach ~85% to the greatest extent during arid periods (Revel et al., 2010). Our sapropel S5 results are consistent with those for S1: cores MS66 and KC20 report a Nile contribution of ~65% and ~55%, respectively, for the detrital sediments (Figure S1). Similar results are obtained while using major elements (Figure S2). Assuming a mixing between Saharan dust and Nile/Aegean contributions for the Levantine Basin, the estimated Nile contribution for these cores are: MS66 (~75%), KC20 (~45%), and KC19 (~5%) (Figure S2).

For the western parts of the EMS, at least a ternary mixing system is needed (Figure S2). For the area south of Crete between ~25 and 30°E, a mixing pattern between Saharan dust, Nile/Aegean, and Libyan contributions can be assumed. As a result, the estimated contributions for the cores (KC19; KC13): Nile (~10%; <5%), Aegean (50–60%; 30–40%), Libyan (<5%; 40–50%), and Saharan (~25%; ~20%) (Figure S2). Notably, core KC19 marks a distribution limit of the Libyan-Tunisian paleodrainage fluxes, and is presumed to have a similar Nile contribution as today (5–10%); while KC13 is suggested to have a negligible Nile influence (see Section 4.2 of the manuscript).

For the northern Ionian Sea (i.e. PS25 and KC01) that is dominated by enhanced NBEM riverine inputs, however, the Adriatic and Aegean contributions cannot be clearly differentiated. In addition, this area may be affected by detrital supplies from Libya, Sicily, and Messina, which makes the Ionian provenance very complex. It seems that the inferred Libyan-Tunisian paleodrainage contributed a small amount of detrital materials to core KC01, but considerably to PS25 (Figures 2 and 3 of the manuscript).

A higher paleodrainage contribution from the Libyan-Tunisian margin must have occurred during sapropel S5 than during S1. This is evidently seen from the Sr-Nd isotopes and major elements (Figures 2 and 3 of the manuscript). Based on a multiproxy approach, the S1 paleodrainage fluxes have been reported to account for 40–70% of the detrital sediments in core CP10/11 (the same site as CP11) (Wu et al., 2017). This is also supported by the estimate (~60%) according to the Sr and Nd isotopes data of sapropel S1 in core CP10 (Wu et al., 2016); for sapropel S5 samples (CP11 and BP22), a similar

three-endmember estimate gives the proportions of 60–75%. Taken together, regardless of other minor detrital contributions and the associated dilution effects, such as the NBEM riverine inputs, shelf-derived fluxes from Sicily, and reduced Saharan dust, a predominant contribution of the S5 paleodrainage flux for the southern Ionian Sea is demonstrated (i.e. ~60–75% contributions for CP11 and BP22 during sapropel S5 time) (Figure S2).

References

Box, M.R., Krom, M.D., Cliff, R.A., Bar-Matthews, M., Almogi-Labin, A., Ayalon, A., Paterne, M., 2011. Response of the Nile and its catchment to millennial-scale climatic change since the LGM from Sr isotopes and major elements of East Mediterranean sediments. Quaternary Science Reviews 30, 431–442.

De Lange, G.J., Thomson, J., Reitz, A., Slomp, C.P., Principato, M.S., Erba, E., Corselli, C., 2008. Synchronous basin-wide formation and redox-controlled preservation of a Mediterranean sapropel. Nature Geoscience 1, 606–610.

Ehrmann, W., Schmiedl, G., Hamann, Y., Kuhnt, T., Hemleben, C., Siebel, W., 2007. Clay minerals in late glacial and Holocene sediments of the northern and southern Aegean Sea. Palaeogeography Palaeoclimatology Palaeoecology 249, 36–57.

Freydier, R., Michard, A., de Lange, G.J., Thomson, J., 2001. Nd isotopic compositions of Eastern Mediterranean sediments: tracers of the Nile influence during sapropel S1 formation? Marine Geology 177, 45–62.

Frost, C., O'Nions, R., Goldstein, S., 1986. Mass balance for Nd in the Mediterranean Sea. Chemical Geology 55, 45–50.

Krom, M.D., Michard, A., Cliff, R.A., Strohle, K., 1999b. Sources of sediment to the Ionian Sea and western Levantine basin of the Eastern Mediterranean during S-1 sapropel times. Marine Geology 160, 45–61.

Revel, M., Ducassou, E., Grousset, F.E., Bernasconi, S.M., Migeon, S., Revillon, S., Mascle, J., Murat, A., Zaragosi, S., Bosch, D., 2010. 100,000 Years of African monsoon variability recorded in sediments of the Nile margin. Quaternary Science Reviews 29, 1342–1362.

Revel, M., Colin, C., Bernasconi, S., Combourieu-Nebout, N., Ducassou, E., Grousset, F.E., Rolland, Y., Migeon, S., Bosch, D., Brunet, P., Zhao, Y.L., Mascle, J., 2014. 21,000 Years of Ethiopian African monsoon variability recorded in sediments of the western Nile deep-sea fan. Regional Environmental Change 14, 1685–1696.

Tachikawa, K., Roy-Barman, M., Michard, A., Thouron, D., Yeghicheyan, D., Jeandel, C., 2004. Neodymium isotopes in the Mediterranean Sea: Comparison between seawater and sediment signals. Geochimica et Cosmochimica Acta 68, 3095–3106.

Weldeab, S., Emeis, K.C., Hemleben, C., Siebel, W., 2002a. Provenance of lithogenic surface sediments and pathways of riverine suspended matter in the Eastern Mediterranean Sea: evidence from $^{143}Nd/^{144}Nd$ and $^{87}Sr/^{86}Sr$ ratios. Chemical Geology 186, 139–149.

Wu, J., Böning, P., Pahnke, K., Tachikawa, K., de Lange, G.J., 2016. Unraveling North-African riverine and aeolian contributions to central Mediterranean sediments during Holocene sapropel S1 formation. Quaternary Science Reviews 152, 31–48.

Wu, J., Liu, Z., Stuut, J.-B.W, Zhao, Y., Schirone, A., de Lange, G.J., 2017. North-African paleodrainage discharges to the central Mediterranean during the last 18,000 years: a multiproxy characterization. Quaternary Science Reviews 163, 95–113.

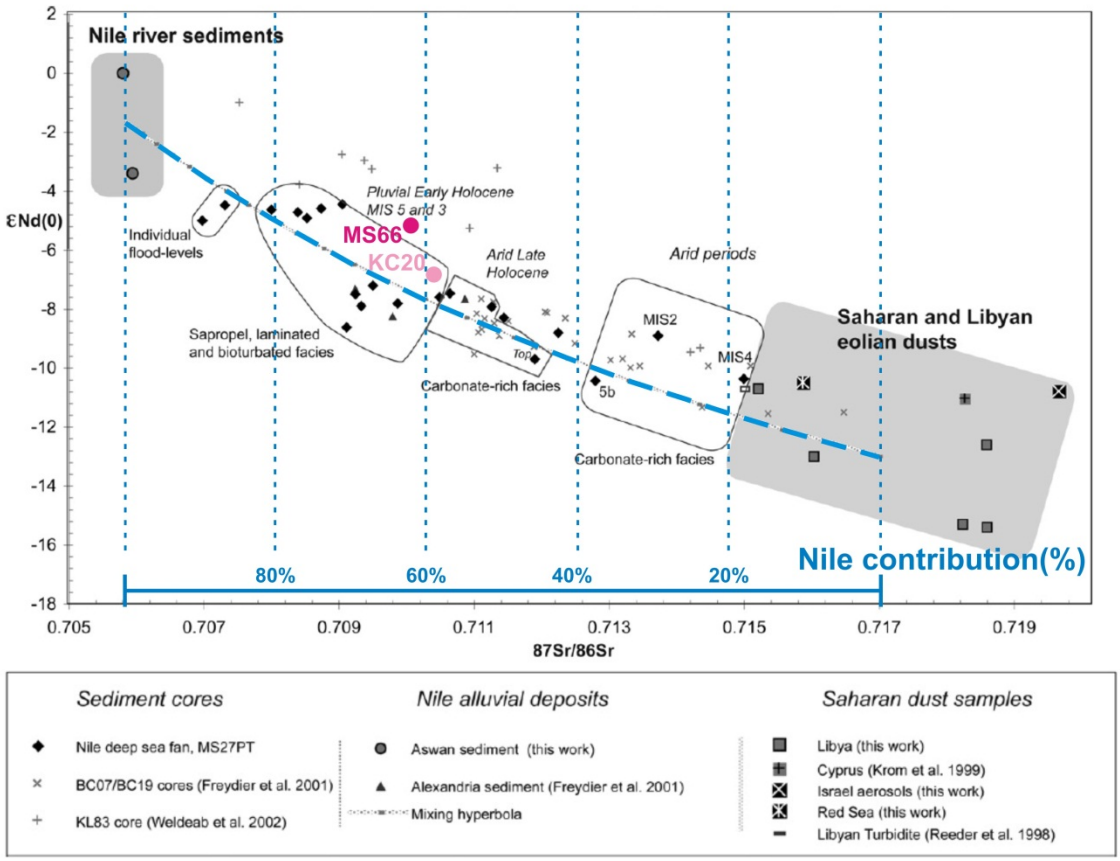

Figure S1

The plot of Sr vs. Nd isotope composition, showing a mixing hyperbola between Nile sediment and Saharan dust for the Levantine Basin (after Revel et al., 2010). This is constructed based on both Sr and Nd isotopes and concentrations, compiled from the various, completed Nile and Saharan samples. Our sapropel S5 samples of cores MS66 and KC20 show a Nile contribution of ~65% and ~55%, respectively, for the detrital sediments.

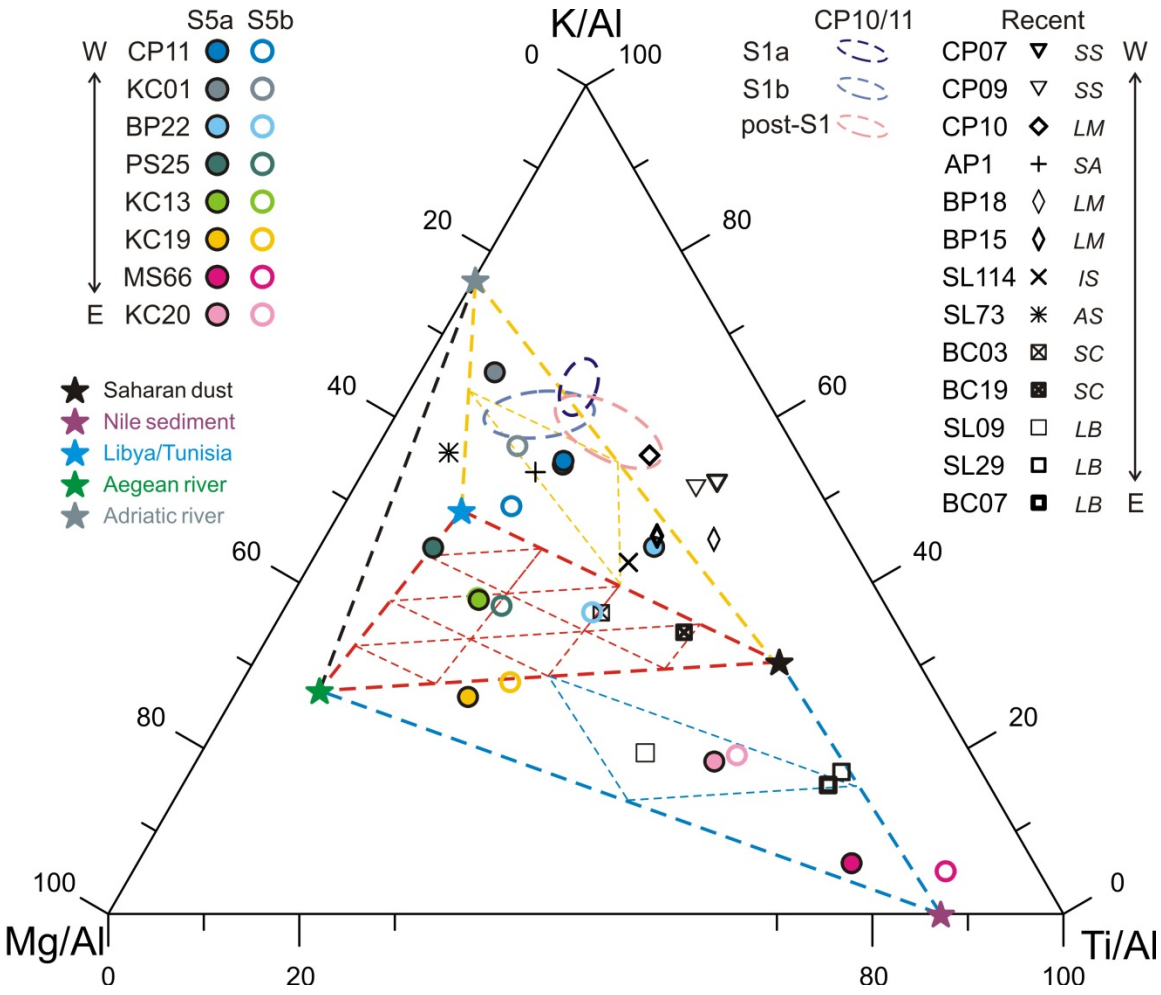

Figure S2

A ternary diagram of major elements in the detrital fraction is used to estimate the detrital contributions during sapropel S5 period (also see Figure 3 of the manuscript). For the Levantine Basin, a mixing between Saharan dust and Nile/Aegean contributions can be assumed (MS66, KC20, and KC19) (blue-triangle area). For the area south of Crete, a mixing between Saharan, Nile/Aegean, and Libyan contributions can be assumed (KC19 and KC13) (red-triangle area). For the northern Ionian Sea (PS25 and KC01), riverine inputs from the Aegean and Adriatic areas must have dominated. For the Libyan-Tunisian margin (CP11 and BP22), paleodrainage fluxes are substantially higher during S5 (60–75%) than during sapropel S1 (40–70%) (yellow-triangle area).

Table S1

Sr and Nd isotope composition of detrital sediments for eastern Mediterranean surface samples

Locality [a]	Core	Latitude, Longitude	Water-depth	$^{87}Sr/^{86}Sr$ $\pm 2\sigma \times 10^{-6}$	$^{143}Nd/144Nd$ $\pm 2\sigma \times 10^{-6}$	ε_{Nd}	Source [b]
SS	CP07	36°02.2'N, 13°06.6'E	524 m	0.716435 ± 10	0.511992 ± 9	-12.5	1
SS	KL60	37°20.2'N, 13°11.3'E	470 m	0.715700 ± 10	0.512017 ± 7	-12.1	2
SS				**0.716068**		**-12.3**	
GM	MC536	37°23.7'N, 16°00.4'E	2850 m	0.720086 ± 10	0.512079 ± 10	-10.9	2
GM	MC533	37°00.2'N, 16°09.4'E	2718 m	0.717931 ± 10	0.512065 ± 9	-11.2	2
GM				**0.719009**		**-11.0**	
SA	MC10	40°08.3'N, 17°01.8'E	1100 m	0.716945 ± 10	0.512123 ± 7	-10.0	2
SA	MC531	39°31.7'N, 18°58.3'E	832 m	0.716887 ± 10	0.512143 ± 9	-9.7	2
SA	MC532	39°56.8'N, 18°60.0'E	910 m	0.717533 ± 10	0.512145 ± 10	-9.6	2
SA	AP1	39°13.0'N, 19°06.8'E	811 m	0.718342 ± 15	0.512033 ± 10	-11.8	3
SA				**0.717427**		**-10.3**	
LM	CP10BC	34°32.7'N, 16°34.0'E	1501 m	0.719740 ± 15	0.512027 ± 16	-11.9	4
LM	BP15	32°46.7'N, 19°52.6'E	665 m	0.718807 ± 11	0.512006 ± 17	-12.2	1
LM				**0.719274**		**-12.0**	
IS	964A	36°15.6'N, 17°45.0'E	3657 m	0.717057 ± 10	0.512015 ± 8	-12.2	2
IS	973A	35°46.8'N, 18°56.9'E	3695 m	0.716977 ± 10	0.512018 ± 8	-12.1	2
IS	KL55	34°18.2'N, 19°53.9'E	3129 m	0.717430 ± 10	0.511995 ± 8	-12.5	2
IS	MC534	35°13.8'N, 21°28.3'E	3515 m	0.715924 ± 10	0.512076 ± 9	-11.0	2
IS	KL59	35°48.6'N, 22°40.2'E	1012 m	0.716473 ± 10	0.512074 ± 8	-11.0	2
IS	SL114	35°17.2'N, 21°24.5'E	3390 m	0.718895 ± 15	0.512019 ± 10	-12.1	3
IS				**0.717126**		**-11.8**	
AS	MC515	39°16.5'N, 23°43.0'E	1250 m	0.713245 ± 10	0.512247 ± 8	-7.6	2
AS	MC521	35°49.0'N, 25°16.0'E	1839 m	0.713724 ± 10	0.512217 ± 9	-8.2	2
AS	MC522	35°50.5'N, 25°26.0'E	1840 m	0.713734 ± 10	0.512206 ± 7	-8.4	2
AS	KL49	36°08.8'N, 25°33.8'E	828 m	0.713831 ± 10	0.512209 ± 10	-8.4	2
AS	KL50	35°36.0'N, 25°54.3'E	560 m	0.710914 ± 10	0.512341 ± 9	-5.8	2
AS	SL123	35°45.3'N, 27°33.3'E	728 m	0.714882 ± 10	0.512186 ± 9	-8.8	5
AS	SL73	39°39.7'N, 24°30.7'E	339 m	0.710380 ± 15	0.512208 ± 10	-8.4	3
AS	MST1	36°10.0'N, 25°12.0'E	1600 m	0.714010 ± 15	0.512248 ± 10	-7.6	3
AS				**0.713090**		**-7.9**	
SC	SL71	34°48.6'N, 23°11.7'E	2827 m	0.716950 ± 10	0.512051 ± 10	-11.5	2
SC	971A	33°43.6'N, 24°40.8'E	2037 m	0.715968 ± 10	0.512070 ± 10	-11.1	2
SC	970A	33°44.2'N, 24°48.1'E	2087 m	0.716211 ± 10	0.512077 ± 10	-10.9	2
SC	KL53	33°51.6'N, 24°51.5'E	2165 m	0.716395 ± 10	0.512067 ± 10	-11.1	2
SC	969A	33°50.5'N, 24°53.0'E	2200 m	0.716119 ± 10	0.512062 ± 7	-11.2	2
SC	RC9-179	34°24.0'N, 27°18.0'E		0.713428 ± 46	0.512172 ± 22	-8.4	6
SC				**0.715845**		**-10.7**	
LB	SL67	34°48.8'N, 27°17.8'E	2157 m	0.714959 ± 10	0.512152 ± 9	-9.5	2
LB	MC21	33°36.3'N, 28°34.3'E	3039 m	0.714361 ± 10	0.512157 ± 8	-9.3	2
LB	MC22	33°14.7'N, 29°27.3'E	2948 m	0.714213 ± 10	0.512150 ± 10	-9.5	2
LB	MC23	32°40.8'N, 30°35.8'E	1940 m	0.710944 ± 10	0.512367 ± 10	-5.3	2
LB	MC24	32°19.5'N, 31°10.5'E	1007 m	0.709495 ± 10	0.512468 ± 9	-3.3	2
LB	MC25	32°00.5'N, 31°53.3'E	199 m	0.708426 ± 10	0.512441 ± 8	-3.8	2
LB	MC38	34°26.1'N, 32°37.6'E	2473 m	0.712306 ± 10	0.512440 ± 10	-3.8	2
LB	966A	33°47.8'N, 32°42.1'E	926 m	0.711386 ± 10	0.512289 ± 8	-6.8	2
LB	968A	34°19.9'N, 32°45.1'E	1961 m	0.710862 ± 10	0.512312 ± 11	-6.4	2
LB	KL85	32°36.8'N, 34°01.6'E	1450 m	0.709381 ± 10	0.512485 ± 10	-3.0	2
LB	KL83	32°36.9'N, 34°08.9'E	1431 m	0.711353 ± 10	0.512472 ± 8	-3.2	2
LB	KL82	32°19.3'N, 34°09.9'E	1284 m	0.709053 ± 10	0.512495 ± 8	-2.8	2
LB	MC35	33°01.6'N, 34°50.6'E	1028 m	0.707531 ± 10	0.512583 ± 10	-1.0	2

LB	MS27PT	31°47.9'N, 29°27.7'E	1389 m	0.711896 ± 10	0.512141 ± 7	-9.7	7
LB	BC07	33°49.4'N, 32°40.0'E	893 m	0.712503 ± 15	0.512167 ± 10	-9.2	8
LB	SL09	34°17.2'N, 31°31.4'E	2302 m	0.713660 ± 15	0.512109 ± 10	-10.3	2
LB	MD84-641	33°02.0'N, 33°38.0'E	1375 m	0.710837 ± 15	0.512325 ± 10	-6.1	3
LB				**0.711363**		**-6.1**	

[a] The locality abbreviations: *SS* = Strait of Sicily, *GM* = Gulf of Messina, *SA* = South Adriatic, *LM* = Libyan-Tunisian Margin, *IS* = Ionian Sea, *AS* = Aegean Sea, *SC* = South of Crete, *LB* = Levantine Basin. Averaged values of $^{87}Sr/^{86}Sr$ and ε_{Nd} are in bold and reported in the paper.

[b] Data sources: 1= this study, 2= Weldeab et al. (2002a), 3= Tachikawa et al. (2004), 4= Wu et al. (2016), 5= Ehrmann et al. (2007), 6= Frost et al. (1986), 7= Revel et al. (2010), 8= Freydier et al. (2001).

Table S2

Sr and Nd isotope compositions of detrital sediments of sapropel S1 over the eastern Mediterranean Sea

Core	Location	Water-depth	$^{87}Sr/^{86}Sr$	ε_{Nd}	Sample number	Source [a]
CP10BC	34°32.7'N, 16°34.0'E	1501 m	0.716120	-11.2	17	1
KC01	36°15.3'N, 17°44.3'E	3643 m	0.713757		3	2
UM42	34°57.2'N, 17°51.8'E	1375 m	0.715710	-11.3	5	3
MP50	39°29.0'N, 18°31.0'E	775 m	0.719415	-9.8	4	4
UM35	35°11.0'N, 21°12.5'E	2670 m	0.715235		4	2
SL114	35°17.2'N, 21°24.5'E	3390 m	0.716071	-10.4	4	1
BC03	33°22.5'N, 24°46.0'E	2180 m	0.716150	-11.0	8	3
ABC26	33°21.3'N, 24°55.7'E	2150 m	0.714827		3	2
MC12 [b]	*~ 33.4°N, 24.9°E*	~2000 m	0.713165		2	2
Stn20 [b]	*~ 34.0°N, 27.5°E*	~2000 m	0.714077		3	2
BC19	33°47.9'N, 28°36.5'E	2750 m	0.712497	-8.7	8	3
MS27PT	31°47.9'N, 29°27.3'E	1389 m	0.707848	-4.9	14	5
BC07	33°40.0'N, 32°40.0'E	893 m	0.711300	-8.4	5	3
9501	34°32.0'N, 33°59.0'E	980 m	0.710616		14	6
9509	32°02.0'N, 34°17.0'E	884 m	0.709375		11	6

[a] Data sources: 1= Wu et al. (2016), 2= Krom et al. (1999b), 3= Freydier et al. (2001), 4= J. Wu (unpublished), 5= Revel et al. (2010; 2014), 6= Box et al. (2011).

[b] Estimated locations and water-depths.